Nature-inspired microfluidic propulsion using magnetic artificial cilia

Khaderi, Syed Nizamuddin

Chapter 3
Asymmetric configurations

Abstract

In this chapter we mimic the efficient propulsion mechanism of natural cilia by magnetically actuating thin films in a cyclic but non-reciprocating manner. By simultaneously solving the elasto-dynamic, magnetostatic and fluid mechanics equations, we show that the amount of fluid propelled is proportional to the area swept by the cilia. By using the intricate interplay between film magnetization and applied field we are able to generate a pronounced asymmetry and associated flow. We delineate the functional response of the system in terms of three dimensionless parameters that capture the relative contribution of elastic, inertial, viscous and magnetic forces.

3.1 Introduction

A rapidly growing field in biotechnology is the use of lab-on-a-chip devices to analyse bio-fluids (Laser & Santiago, 2004; Whitesides, 2006; Chang *et al.*, 2007). Such fluids have to be preprocessed (for example, mixed with other fluids (den Toonder *et al.*, 2008)) and transported to and from one or many micro-chambers where the biochemical analyses are performed. The microfluid transport through these stages is usually performed by downscaling conventional methods such as syringe pumps (Schilling *et al.*, 2002; Jeon *et al.*, 2000), micropumps (Laser & Santiago, 2004), or by exploiting electro-magnetic actuation, as in electro-osmotic (Zeng *et al.*, 2002; Chen *et al.*, 2003) and magnetohydrodynamic devices (Lemoff & Lee, 2000; Homsy *et al.*, 2000). However, when transporting biological fluids (which usually have high conductivity), the use of electric fields may induce heating, bubble formation and pH gradients from electrochemical reactions (Studer *et al.*, 2004; Wu *et al.*, 2007; Bruss *et al.*, 2004). In this chapter, we explore a new way to manipulate fluids in microfluidic systems, inspired by nature, through the magnetic actuation of artifical cilia.

Fluid dynamics at the micrometre scale is dominated by viscosity rather than inertia. This has important consequences for fluid propulsion mechanisms (Purcell, 1977). In particular, mechanical actuation will only be effective in propelling fluids if their motion is cyclic, but asymmetric in shape change. Nature has solved this problem by means of hair-like structures, called cilia, whose beating pattern is asymmetric and consists of an effective and a recovery stroke (Murase, 1992). While natural cilia use an internal forcing system based on motor proteins (dyneins), the key challenge for its artificial equivalent

Based on Khaderi, *et al. Nature-inspired microfluidic propulsion using magnetic actuation*, Physical Review E, 2009, **79**, 046304.

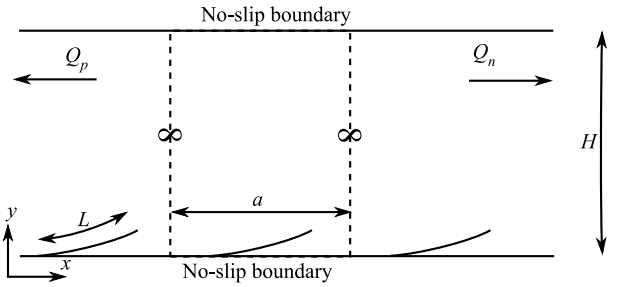

Figure 3.1: *Schematic side view of the microfluidic channel used in the simulations. The unit-cell used is shown using dashed lines.*

is the design of an externally-applied loading system that will generate a similar non-reciprocating motion. Recently, electrostatic artificial cilia have been experimentally shown to induce effective micro-mixing (den Toonder *et al.*, 2008). In addition, magnetic fields are also used to induce flow, but the asymmetry generated was found to be relatively small (Gauger *et al.*, 2009). In this chapter we report on the identification of four magnetically-driven configurations that can exhibit an asymmetric motion. We will show that the fluid propelled is linearly proportional to the swept area by the film (the configurational space). The first configuration is based on a partially magnetic film that can have different stiffnesses during the effective and recovery stroke. The next two are based on a magnetic instability that develops when the applied magnetic field is opposite to the direction of the magnetization in a permanently magnetic film. In the fourth configuration we will demonstrate that asymmetry can be achieved in a super-paramagnetic film, based on the intricate inter-play between the geometry of the film, the externally-applied field and the induced magnetization.

3.2 Results

We use the numerical model developed in chapter 2 to study a periodic arrangement of cilia in a microfluidic channel of height $5L$, with the cilia spaced $5L$ apart in the limit of low Reynolds numbers, where L is the length of the cilia. A square unit-cell is identified consisting of one cilium. No-slip boundary conditions are applied at the top and bottom boundaries of the channel and periodic boundary conditions at the left and right ends of the unit-cell (see Fig. 3.1). The fluid has a viscosity $\mu = 1$ mPas. The film has a thickness $h = 2$ μm, an elastic modulus of 1 MPa and a density $\rho = 1600$ kg/m^3, unless mentioned otherwise. In the following, the Eulerian fluid mesh is not shown for clarity.

3.2.1 Partly magnetic film with cracks.

Early studies on the mechanical properties of a cilium, when no information on the microstructure was available, showed that the natural cilium has a larger stiffness during the effective stroke compared to the recovery stroke (Gray, 1922). Because of the large stiffness, the cilium does not deform during the effective stroke, while due to the low stiffness the drag forces cause the cilium to deform considerably so that it stays closer to the cell boundary during the recovery stroke. To use this concept the magnetic film needs to possess a large bending stiffness in the effective stroke while pushing the fluid and to

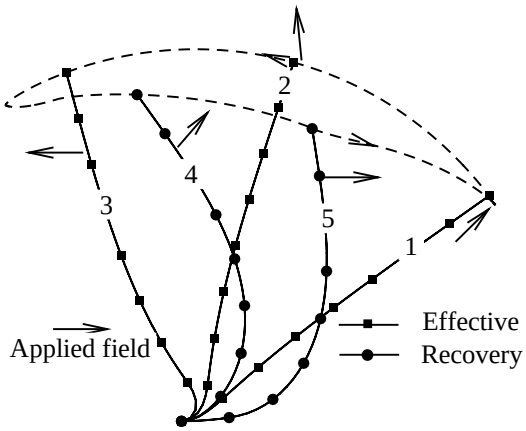

Figure 3.2: *Film with cracks with only a part (20% of the length) near the fixed end magnetized. Instances 1, 2, 3, 4 and 5 refer to a time of 5, 11, 20, 27 and 30 ms, respectively. The arrows show the direction of the applied field.*

possess a low stiffness during the recovery stroke. This can be achieved by introducing cracks on one side of the film and by making only a portion of the film magnetic. The film, which is straight initially, is attached at the left end and has cracks of size 1 μm at the bottom. As only a part of the film is magnetic, it behaves like a flexible oar (as also mentioned by Purcell (1977)). Only 20% of the film near the fixed end is magnetic. The assumed remnant magnetization is 15 kA/m, with the magnetization vector pointing from the fixed end to the free end. The applied magnetic field ($B_0 = 75$ mT) initially points in the positive x-direction, after which it is rotated by 180° in the counterclockwise direction in 20 ms and then rotated back to the initial position in the next 10 ms, thereafter this cycle is repeated. The movement of the film under the action of the applied magnetic field is shown in Fig. 3.2. When the external magnetic field is applied, for the first 20 ms, the magnetic couples act on the magnetized portion of the film in a counterclockwise manner. The drag forces are acting on the top part of the film, which close the cracks and make the film stiff. The cilium thus remains nearly straight and rotates about the fixed end to perform the effective stroke (see instances 1, 2 and 3 in Fig. 3.2). When the applied field rotates back to the initial position during the next 10 ms, the drag forces act on the bottom part of the film which open the cracks making the film floppy and bend it (see instances 4 and 5 in Fig. 3.2). Such an interaction of magnetic couples, elastic forces and drag forces leads to an asymmetric motion, as can be seen from Fig. 3.2.

3.2.2 Buckling of a straight magnetic film

In this configuration, a straight horizontal magnetic film with a perturbation is used to achieve an asymmetric motion. The film considered here has a uniform remanent magnetization of 15 kA/m with the direction of magnetization pointing from the fixed end of the film to the free end. When an external magnetic field is applied in the direction opposite to the film's magnetization, there will be no resulting magnetic couple when the

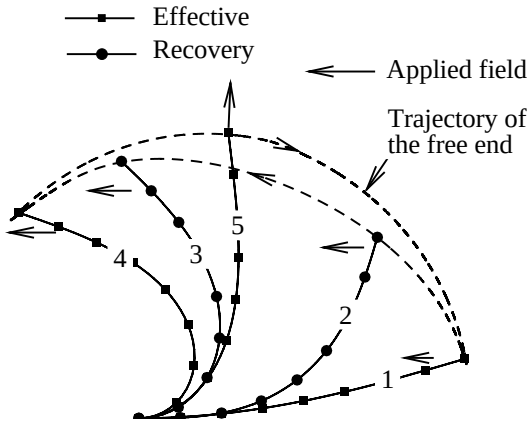

Figure 3.3: *Asymmetric motion of a perturbed permanently magnetic film. The magntization points from the fixed to free end. During instances 1 and 2, the cilium buckles and exhibits a recovery stroke and during instances 3, 4 and 5 it performs effective stroke. Instances 1, 2, 3, 4 and 5 correspond 2, 10, 12, 15 and 20 ms, respectively.*

film is straight, hence the film will not move. However, if the film is not initially straight but given an initial perturbation, due to, for instance, manufacturing imperfections, then it will buckle under the influence of the external magnetic field. By assuming a uniform magnetization in the film and neglecting drag forces, the critical magnetic field that will cause buckling can be calculated (see Appendix I). Figure 3.3 shows the asymmetric motion due to the buckling of a magnetic film. The length of the film is 100 microns. The external magnetic field is linearly increased from zero to a maximum of B_0 (25 mT) in the direction opposite to the magnetization in the film in 15 ms. Then it is rotated by 180° degrees in the clockwise direction in the next 15 ms, after which it is reduced to zero in the next 1 ms and the cycle is repeated. At instant 1 in Fig. 3.3 when the film is nearly horizontal the magnitude of the counterclockwise magnetic couple acting on the film is low. Under the influence of this magnetic couple, the film buckles to instances 2 and 3 and performs the recovery stroke. When the applied field is rotated by 180° in the clockwise direction, the film follows the applied field to perform the effective stroke and comes back to the initial position (instances 4 and 5). The effective fluid propulsion takes place when the film returns to the initial position.

3.2.3 Curled permanently magnetic film

The effect of the buckling-induced recovery stroke can be enhanced by choosing the initial geometry of the film to be a quarter of a circle with radius 100 μm, see instant 1 in Fig. 3.4(a). The direction of the magnetization is along the film with the magnetization vector pointing from the fixed end to the free end. The remanent magnetization of the film is taken to be $M_r = 15$ kA/m. A uniform external field of magnitude $B_0 = 13.3$ mT is applied at 225° to the x axis from $t = 0$ ms to $t = 1$ ms and then linearly reduced to zero in the next 0.2 ms. The results of the non-reciprocating motion of the film in the fluid during magnetic actuation are shown in Fig. 3.4(a). When the external field is

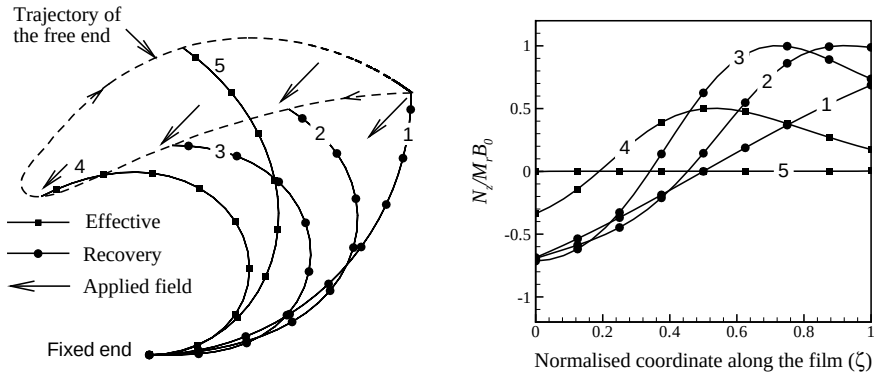

(a) (b)

Figure 3.4: *Buckling of a curled permanently magnetic (PM) film as a result of magnetic actuation, during the propulsion of fluid. (a) Snapshots of the film at 0 ms, 0.3 ms, 0.6 ms, 1.1 ms and 3 ms. (b) Normalised torque distribution along the film corresponding to the snapshots shown in (a).*

applied, clockwise torques (N_z is the magnetic body torque) are acting on the portion near the fixed end of the film while near the free end counter-clockwise torques develop (see instance 1 in Fig. 3.4(b)). Under the influence of such a system of moments, the film undergoes a buckling-kind of instability. This can be nicely seen from instances 1 and 2 in Figs. 3.4(a) and 3.4(b). During this stage the position of zero torque is almost fixed, while the torques at the free end increase. This causes the film to snap through to configurations 3 and 4 during which the zero-torque position travels to the fixed end. Clearly, the initially opposing directions of the internal magnetization and the applied magnetic field are essential in generating an instability that causes a large bending deformation during application of the field. Then, the applied field is reduced to zero and the film returns to the initial position through instance 5 in Fig. 3.4(a). Note that the propulsive action in the effective stroke (red) takes place during the elastic recovery of the film, while the film stays low in the recovery stroke due to the buckling-enforced snap-through.

3.2.4 Super-paramagnetic film

For a PM film the torques are maximum when the local magnetic film is perpendicular to the (remanent) magnetization. For a super-paramagnetic (SPM) film, however, the magnetization is induced by the field itself, posing different requirements on the applied magnetic fields in order to deform the film. A straight, magnetically anisotropic SPM film (having susceptibilities 4.6 and 0.8 in the tangential and normal directions, respectively (van Rijsewijk, 2006)), is subjected to a magnetic field with magnitude $B_0 = 31.5$ mT that is rotated from 0° to 180° in $t = 10$ ms and then kept constant during the rest of the cycle. The film has a length $L = 100$ μm. Its cross-section is tapered, with the thickness varying linearly along its length, having $h = 2$ μm at the left (attached) end and $h = 1$ μm at the right end. Figure 3.5(a) shows that in the effective stroke the portion of the beam near the free end is nearly straight. This is due to the fact that in this region

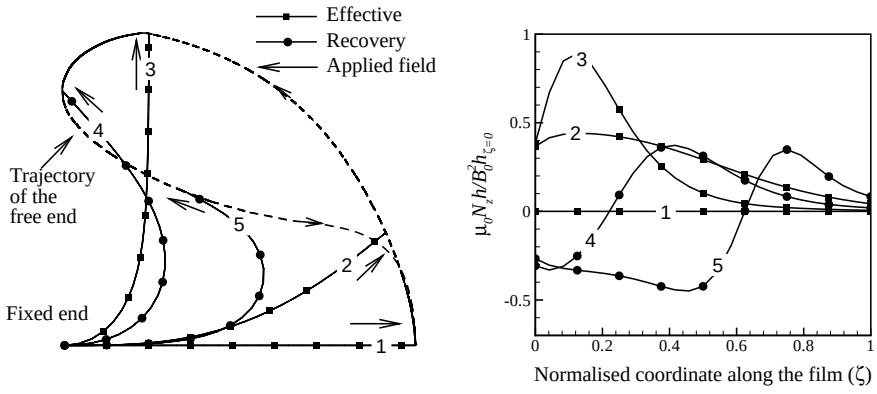

(a) (b)

Figure 3.5: *Motion of a super-paramagnetic (SPM) film in a rotating magnetic field, during the propulsion of fluid. (a) Snapshots of the film at 0 ms, 2.5 ms, 5.0 ms, 7.5 ms and 8.5 ms. (b) Normalised torque distribution along the film corresponding to the snapshots shown in (a). Here μ_0 is the permeability of vacuum, h is the thickness at position ζ and $h_{\zeta=0}$ is the thickness at the fixed end.*

the film can easily follow the applied field so that the field and magnetization are almost parallel, causing the magnetic torque to be low in this region of the film (instances 2, 3 and 4 in Fig. 3.5(b)). When the film has reached position 4, the magnetization in the film is such that the torques are oriented clockwise near the fixed end and anticlockwise near the free end, resulting in strong bending of the film. From Fig. 3.5(b) it can be seen that during the recovery stroke (shown using circles) the position of zero torque propagates from the fixed end to the free end (from instance 4 to 5). Here the tapering is essential, causing the torque per unit length to be higher at the fixed end, allowing the film to recover to the initial position (1). The generated asymmetric motion is very similar to that of natural cilia (Murase, 1992). It is to be noted that the film recovers in the presence of an applied magnetic field. This sensitive interplay between stored elastic energy and controlled applied field can be exploited to provide a large asymmetry in motion.

3.2.5 Fluid propelled

Next we analyse how much fluid is propelled by the cilia. The asymmetry is large only in the cases of the curled permanently magnetic film and tapered super-paramagnetic film; hence, we analyse only these cases. We record the fluid volume transported through the channel per cycle and per unit out-of-plane thickness, giving an area flow per cycle (or volume flow per unit width). As a measure for the asymmetry, we compute the area swept by the free end of the film during one cycle (i.e. the area enclosed by the dashed lines in Figs. 3.4(a) and 3.5(a)) and vary this area by tuning the magnitude of the applied magnetic field (all other parameters remain unchanged). Figure 3.6 shows the area flow per cycle as a function of the swept area for several different cases. We have normalised both quantities by the maximum area that the tip can sweep, $\pi L^2/2$. For three values of the magnetic field we plot the film tip trajectories for the PM and

SPM configurations. The cycle times are 35 and 10 ms, respectively. The flux across the channel shows a linear dependence on the swept area. A similar result has been reported by Golestanian & Ajdari (2008) where it is shown that the velocity of a three sphere swimmer is proportional to the area swept in the configurational space. Due to

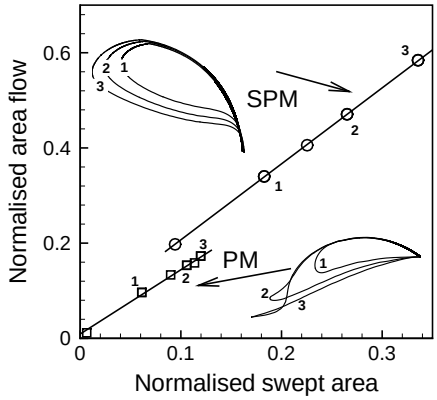

Figure 3.6: *Variation of normalised area flow with swept area.*

the linear correlation between the swept area and the fluid flow, the swept area can be used as a measure of effectiveness of the actuator, representing the fluid volume displaced. This allows uncoupling the magneto-mechanical motion of the cilia from the computationally-intensive fluid dynamics calculations. Instead, we account for the fluid by means of velocity-proportional drag forces (using resistive force theory (Johnson & Brokaw, 1979)) on the cilia, with the drag coefficients calibrated to the coupled solid-fluid model (see appendix H).

3.2.6 Parametric study

To identify the dimensionless parameters that govern the behaviour of the system, we start from the virtual work equation for the film , neglecting the axial deformations:

$$\int EI\frac{\partial^2 v}{\partial x^2}\frac{\partial^2 \delta v}{\partial x^2}dx + \int \rho A\frac{\partial^2 v}{\partial t^2}\delta v dx - \int N_z\frac{\partial \delta v}{\partial x}Adx + \int C_y\frac{\partial v}{\partial t}\delta v b dx = 0, \qquad (3.1)$$

where $I = bh^3/12$ is the second moment of area with b the out-of-plane thickness, $A = bh$ is the cross-sectional area of the film and v is the transverse displacement. In the virtual work equation the first, second, third and last terms respectively represent the virtual work done by the elastic internal bending moments, the inertial forces, the magnetic couple and the fluid drag forces. We introduce the dimensionless variables V, T and X, such that $v = VL$, $x = XL$ and $t = Tt_{\text{ref}}$, where L is a characteristic length (taken to be the length of the film) and t_{ref} a characteristic time. Substitution of these variables in the virtual work equation and normalisation with the elastic term reveals the three governing dimensionless numbers: the inertia number, $I_n = 12\rho L^4/Eh^2t_{\text{ref}}^2$, i.e. the ratio of inertial to elastic force, the magnetic number $M_n = 12N_zL^2/Eh^2$, i.e. the ratio of magnetic to elastic force and the fluid number $F_n = 12C_yL^4/Eh^3t_{\text{ref}}$, the ratio of fluid to elastic force. By substituting the torque expression for the two different magnetic materials,

the magnetic number M_n for the PM film is linear in the applied field, $12M_rB_0L^2/Eh^2$, while for the SPM film it is quadratic, $12B_0^2L^2/\mu_0Eh^2$.

We proceed by exploring the functional response of the system in terms of the swept area and cycle time, in dependence of the three dimensionless parameters. We analysed many different combinations of I_n, M_n and F_n, the results of which are summarized in Figs. 3.7(a)-3.7(c) for the PM system and in Figs. 3.7(d)-3.7(f) for the SPM system. Figs. 3.7(a) and 3.7(d) show the swept area as a function of M_n for several combinations of I_n and F_n. The combinations are indicated by the different symbols, corresponding to specific locations in Figs. 3.7(b) and 3.7(e). The effect of all three parameters can also be nicely summarised by analysing what magnetic number and cycle time is needed to sweep a normalised area of 0.2, for a given range of I_n and F_n values (see Figs. 3.7(b), 3.7(c), 3.7(e), 3.7(f)). The swept area increases with M_n reaching a maximum of 0.4 for the PM system (see Fig. 3.7(a)), while values of 0.7 can be reached by the SPM system (see Fig. 3.7(d)). For both systems the M_n needed strongly increases with F_n. In other words, for a given elastic parameter set, larger magnetic forces are needed to overcome the drag forces imposed by the fluid (see Figs. 3.7(a), 3.7(b), 3.7(d) and 3.7(e)). It can be seen from Figs. 3.7(a) and 3.7(d) that the effect of F_n is gradual for the PM system, while for the SPM case it is absent for small F_n, but suddenly kicks in for F_n larger than 10. In addition, the inertial forces assist in generating asymmetry for both cases, although for the SPM system inertial effects are only triggered for very large fluid numbers (see Fig. 3.7(d)).

For the analysis of the normalised cycle time the reference time was taken to be the time during which the field was applied (PM) or rotated (SPM). It was observed that the cycle time dependence on M_n and I_n was very weak and mostly completely absent. The only clear dependence found was on F_n which we show in the inset of Figs. 3.7(a) and 3.7(d) in terms of the normalised cycle times averaged over all different M_n values analysed and in Figs. 3.7(c) and 3.7(f) as the time required to sweep a normalised area of 0.2. For the PM case the effective stroke is generated through the elastic recovery of the deformed film, without noticeable effect of inertial forces. For such overdamped systems the time taken by the system to return to the initial position scales linearly with F_n, the ratio of fluid to elastic forces. The variation of normalised cycle time with F_n for the SPM case is much smaller. This is due to the fact that the total cycle is performed in the presence of magnetic forces. For small F_n and I_n the mean normalised cycle time (see Fig. 3.7(f)) is approximately equal to one; only for large F_n and I_n the cycle time is increased. At large F_n the system relies on the recovery (going from instance 5 to instance 1 in Fig. 3.5) of the curved tip against high viscous forces (see Figs. 3.7(d), 3.7(f)). The systems demonstrate an underdamped behaviour at large I_n values causing inertial forces to generate large oscillations leading to a larger normalised time (see Fig. 3.7(f)). For a normalised area of 0.2 the response of both systems in the range $I_n < 0.1$ and $F_n < 10$ is quasi-static, i.e. independent of inertial and viscous effects.

3.3 Summary

To summarize, we have proposed and analysed magnetic artificial cilia which can transport fluid in microfluidic channels. The main result is that we have found four actuation mechanisms, of which two can display a pronounced asymmetric motion. One configu-

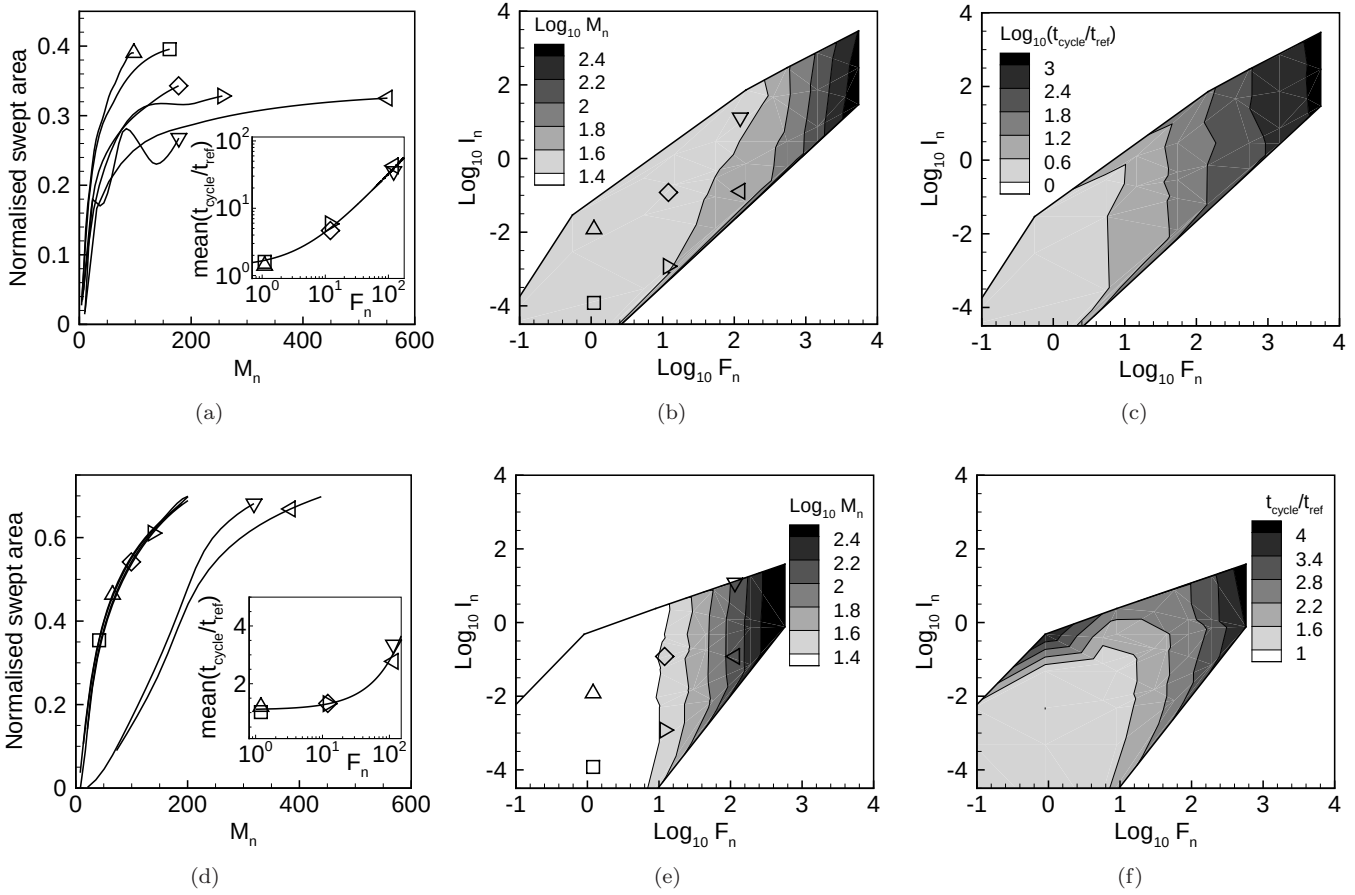

Figure 3.7: *Functional response of the PM system (top row, (a)-(c)) and the SPM system (bottom row, (d)-(f)). (a) (d) Normalised swept area as a function of M_n for several combinations of I_n and F_n, corresponding to the symbols of Figs. (b) and (e). The inset shows the mean normalised cycle time as a function of F_n. The mean is obtained by averaging all times corresponding to the data points that make up the specific M_n-swept area curve. (b) (e) Contours of M_n needed to sweep a normalised area of 0.2 for a wide range of I_n and F_n values. (c) (f) Contours of normalised cycle time corresponding to (b) and (e).*

ration is based on the buckling of a permanently magnetic film and the other is based on the intricate interaction between the applied field and the magnetization in a superparamagnetic film. We have shown that the fluid propelled is linearly proportional to the area swept by the film, which has so far only been shown for a non-actuated kinetic system (Najafi & Golestanian, 2004). Finally, we have identified the range of dimensionless parameters for which the artificial cilia exhibit an optimal behaviour. The analysis presented can be used as a guideline to make artificial cilia for microfluidic transport in lab-on-a-chip systems.